Intrinsic and Extrinsic Analysis on Computational Anatomy

Anqi Qiu, Laurent Younes, Michael I Miller

Intrinsic and Extrinsic Analysis on Computational Anatomy

Anqi Qiu[1], Laurent Younes[1], Michael I. Miller[1]

Center for Imaging Science, The Johns Hopkins University

Abstract. We present intrinsic and extrinsic methods for studying anatomical coordinates in order to perform statistical inference on random physiological signals F across clinical populations. To do so, we introduce generalized partition functions of the coordinates, $\psi(x), x \in \mathcal{M}$, which are used to construct a random field model of F on $\mathcal{M}$. In the intrinsic analysis, such partition functions are defined intrinsically for individual anatomical coordinate based on Courant's theorem on nodal analysis via self adjoint operators. On the contrary to the intrinsic method, the extrinsic method needs only one set of partition functions for a template coordinate system, and then applied to each anatomical coordinate system via transformation. For illustration, we give clinical studies on cortical thickness for each of these methods.

1 Introduction

Computational Anatomy (CA) [1] is a discipline which is evolving rapidly worldwide. The three major areas in CA (i) construction of anatomical manifolds, (ii) metric comparison of anatomical manifolds, and (iii) large deviation testing and statistic inference are proceeding in many groups concurrently. This paper discusses two approaches to statistical inference in disease populations on anatomical manifolds, what we shall term intrinsic and extrinsic methods.

The specificity of the statistical analysis on anatomical manifolds comes from the fact that each observation consists of a physiological signal, F, defined on a manifold, $\mathcal{M}$, which is subject dependent. We refer to the observed signal , $F(x), x \in \mathcal{M}$ as the signal in anatomical coordinates. There are numerous examples, like functional activity, or cortical depth on brain surfaces, fiber orientation from DTI images etc.

To accommodate a statistical analysis, the most general approach is to consider that the observations arise from an infinite dimensional random process $(\mathcal{M}, F)$ that includes the manifold and the physiological observation that is carried by it. The anatomical part of the process $(\mathcal{M})$ can have important clinical implications, and its variations have been showed to be related to pathological states (e.g. [2, 3]). However, our focus is on the analysis of the variations of the physiological signal, F, independently from the anatomical variation that is considered as a nuisance component of the process. The question is how to characterize group differences in F that subsist disregarding variation in the anatomy.

A natural construction for the distribution of $(\mathcal{M}, F)$ is to first model the anatomical part, $\mathcal{M}$, then the physiological part conditional to $\mathcal{M}$. The latter distribution therefore models a random field on $\mathcal{M}$. In this paper, we will consider representations of this random field by a possibly infinite number of random variables given by

$$F_i = \int_{\mathcal{M}} F(x)\psi_i(x)ds(x) \tag{1}$$

where s is the volume form and ψ_i is a function on $\mathcal{M}$. The functions $\psi_1, \psi_2, \ldots$ obviously depend on $\mathcal{M}$, but we will assume that they are completely specified by it (they are deterministic for the conditional distribution given $\mathcal{M}$). We shall refer to them as *generalized partition functions* of the manifold of $\mathcal{M}$. A simple case can be associated to the decomposition model $F(x) = \sum_i F_i\psi_i(x)$ where the ψ_i form an orthonormal basis of $L^2(\mathcal{M})$. They can also be a simple set of indicator functions, leading to a real decomposition of F on a partition. We do not assume here that the representation $F_1, F_2, \ldots$ is exact (i.e., that F can be reconstructed from it), but we expect that it will conserve the necessary information to perform statistical analysis, that will amount to performing inference on the random physiological measurements reduced to the coefficients $F_i, i = 1, 2, \ldots$. The real challenge here is of course the construction of the generalized partition ψ in anatomical coordinates (i.e., defining $\psi_1, \psi_2, \ldots$ from $\mathcal{M}$), and to ensure that the construction is done so that the features F_i retain comparable qualitative interpretation across multiple individuals $\mathcal{M}^{(1)}, \ldots, \mathcal{M}^{(n)}$. Such an approach will be called an *intrinsic analysis*, because it relied on computation that only depend on the observation $(\mathcal{M}, F)$.

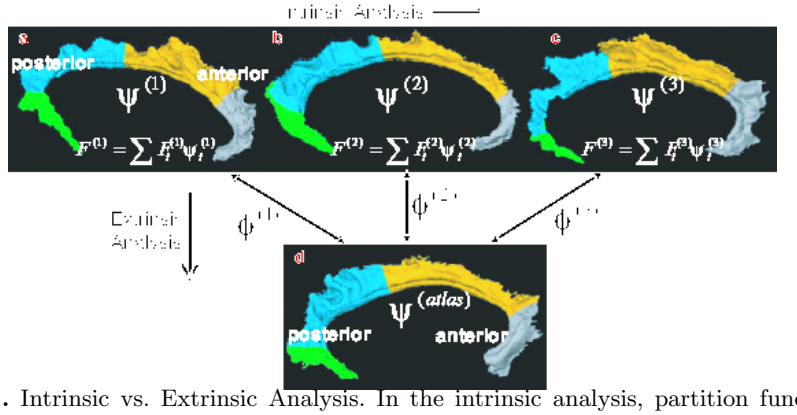

Fig. 1. Intrinsic vs. Extrinsic Analysis. In the intrinsic analysis, partition functions $\psi^{(j)}$ are constructed independently for individual anatomical coordinates shown in panels (a-c). In extrinsic analysis, only one partition function is needed for template coordinates shown in panel (d) and partition functions of other anatomical coordinates are carried onto the template coordinate through mapping ϕ.

We shall develop an example of intrinsic analysis, and also compare it to template based methods that we and many groups (e.g. [4–6]) have been following in the past 10 years. As shown in Figure 1, for each anatomical configuration $\mathcal{M}$ there is a correspondence ϕ which carries the template coordinates

to the anatomy. The implicit statistical model in this framework is that $\mathcal{M}$ is a (random) deformation of the template $\mathcal{M}_{atlas}$. In the approach we have used extensively, this deformation is modeled as a diffeomorphism ϕ of the ambient space (an open subset of $\mathbb{R}^3$), such that $\mathcal{M} = \phi(\mathcal{M}_{atlas})$. The random process F is then pulled back to $\mathcal{M}_{atlas}$ by the transformation $F \rightarrow F \circ \phi$ (the later being defined on the template). It is the pulled-back version that is modeled as a random field on the fixed set $\mathcal{M}_{atlas}$, making its statistical analysis much easier. To define the generalized partition model, one starts with defining $\psi_1, \psi_2, \ldots$ once for all on $\mathcal{M}_{atlas}$, and, given an observation $(\mathcal{M}, F)$, compute the coefficient F_i by first estimating the registration ϕ such that $\mathcal{M} = \phi(\mathcal{M}_{atlas})$, then setting

$$F_i = \int_{\mathcal{M}_{atlas}} F \circ \phi(x)\psi_i(x)ds(x). \tag{2}$$

The power of this approach is of course that only one partition needs to be created, indexed over the template. We call this approach *extrinsic* analysis, since it depends on the relation between the observation and the template. The issues that can be raised on such an approach are that the resulting features depend on the choice of the template, and on the computed correspondences ϕ. The difficulty with this strategy is that for many anatomical configurations the correspondence may not be well defined. For highly curved surfaces in the cortex, the additional transformation required by the mappings may itself introduce errors which can directly influence the statistics being inferred. The results of the analysis may therefore depend on the *algorithm* that is used for estimating ϕ.

For this reason, it is attractive if possible to be able to study variations in the structure and function associated with anatomical coordinates without having to generate these bijective correspondences, that is, to use the *intrinsic* analysis. We provide such an approach in section 3, based on a classical theorem from Courant on nodal analysis and the partition of domains based on self adjoint operators.

An intrinsic approach should address several principles that sustain its well-foundness and efficiency.

1. Intrinsicality: the generalized partition functions ψ_j must be obtained directly from the anatomical coordinates as shown in Figure 1 (a-c), without the availability of the common extrinsic template coordinates and correspondence.
2. Reliability: the functions ψ_j computed from similar manifolds must also be similar.
3. Locality: to be able to obtain statistical conclusions that concern specific regions of the manifold, the functions ψ_j must be supported by a subregion of $\mathcal{M}$.

2 Intrinsic and Extrinsic Random Field Models

An interesting illustration of the difference between the intrinsic and extrinsic approaches comes from the two random field models they respectively lead to.

Intrinsic Model. Denote $L^2(\mathcal{M})$ for the set of square integrable functions on $\mathcal{M}$. Let $\psi^{\mathcal{M}} = (\psi_1, \psi_2, \ldots)$ form an orthonormal basis of $L^2(\mathcal{M})$. Then, the conditional distribution of F given $\mathcal{M}$ can be defined via the decomposition

$$F = F_0 + \sum_{k=1}^{\infty} F_k \psi_k,$$

F_0 being a given, average function, and $F_1, F_2, \ldots$ being uncorrelated Gaussian variables of respective variances $\sigma_1^2, \sigma_2^2, \ldots$. Such models have been considered in [7], with the ψ_i being the eigenfunctions of the Laplace-Beltrami operator on $\mathcal{M}$.

Extrinsic Model. In the extrinsic approach, modeling focuses on the template. Defining $\psi^{atlas} = (\psi_1, \psi_2, \ldots)$ to be an orthonormal basis of $L^2(\mathcal{M}_{atlas})$, one can model a function F defined on $\mathcal{M} = \phi(\mathcal{M}_{atlas})$ by

$$F = F_0 \circ \phi^{-1} + \sum_{k=1}^{\infty} F_k \psi_k i \circ \phi^{-1}$$

with independent F_k. Equivalently, the model is that the registered physiological measure, $F \circ \phi$ follows a distribution (as a random field on $\mathcal{M}_{atlas}$) similar to the intrinsic distribution we have discussed above.

It is a powerful tool for analyzing brain function, and has successfully been used by several groups including ours (e.g. [2, 3]). It is robust, since the choice of the basis ψ is done once for the atlas, and then transported to the observed manifolds. As we have already noticed, however, one important drawback is that the model depends on the registration ϕ which is not observed. It therefore depends on the implemented registration algorithm: different algorithms yield different models and possibly different conclusions.

This last drawback is, by construction, absent from the intrinsic approach. The issue there is that, since the ψ_i are computed independently for each manifold, it is not sure that they can be given a universal interpretation on a given class of observations (on cingulates, or planum temporale, for example). Even if the distribution of F can be assumed to be robust as a whole (by letting, in the case of a decomposition of the Laplace-Beltrami operator, the variance of F_i be a fixed function of the eigenvalue associated to ψ_i), it is not always the case for the computed values of F_i. This robustness depends on fact on the considered class of manifolds, as will be illustrated later.

Both the intrinsic and extrinsic constructions above are unsatisfactory, however, because they do not address the locality constraint that is desirable for the interpretability of the results. We now describe how the eigenfunctions of the Laplacian can be used to define intrinsic regions on the manifolds, through the notion of nodal decomposition. Nodal decomposition based on the Laplacian has been used in other areas, such as image segmentation, graph decomposition, et al. [8–10]. Moreover, the Laplace-Beltrami operator has been used in the brain studies, such as surface and function smoothing, conformal mapping [7, 11–13]

3 Intrinsic Study of Anatomical Coordinates

To generate an intrinsic partition, we start with a classical result from Courant on the partition of coordinates based on nodal domains. The nodal (or zero-crossing) lines of the eigenfunctions of a self-adjoint operator defined on the manifold separates it in a partition with a predictable number of connected components. We are particularly interested in cortical surfaces for our partition.

Courant's nodal theorem [14]: *Let L be a self adjoint differential operator and consider the differential equation $L\psi + \lambda\psi = 0$, for a domain $\mathcal{M}$ with arbitrary homogeneous boundary conditions; if its eigenfunctions are ordered according to increasing eigenvalues, then the nodes of the ith eigenfunction ψ_i divide the domain into no more than i subdomains. No assumptions are made about the number of independent variables.*

Such subdomains are called *nodal domains*. Lines where ψ_i changes sign are defined as *nodal lines*. On a triangulated mesh, ψ_i is defined on each vertex of the mesh. It may change from positive to negative without passing through zero. The discrete analogue of a *nodal domain* is a connected set of vertices on which the eigenfunction has the same, strict or loose, sign. For our partition we

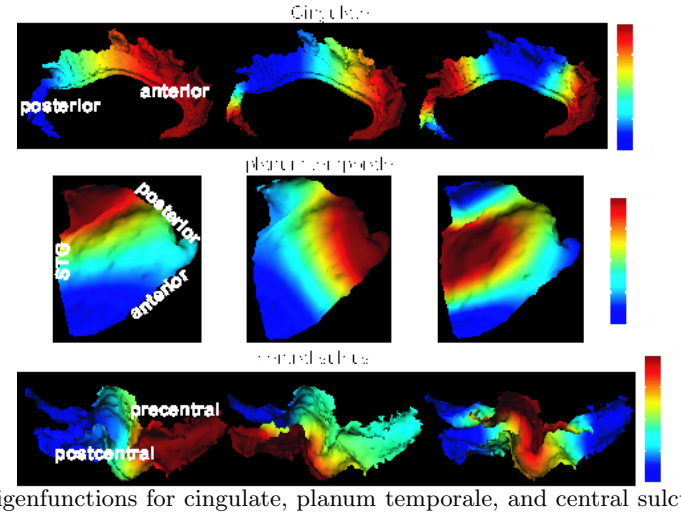

Fig. 2. Eigenfunctions for cingulate, planum temporale, and central sulcus are shown from top to bottom. The second, third, and fourth eigenfunctions are shown from left to right.

follow our previous work [7] deriving them as an orthonormal basis constructed from the Laplace-Beltrami (LB) operator, which is the extension of the Laplace operator from a regular grid to an arbitrary surface. The LB incorporates the intrinsic geometric properties of a surface, such as angle between two curves on the surface, length of a curve, and area, so that subregions of the cortical surface defined by the LB eigenfunctions are based on the geometric information of the cortex itself.

The LB spectral problem with Neumann boundary conditions for surface $\mathcal{M}$ is posed as

$$\begin{aligned} \Delta\psi(\mathbf{u}) + \lambda\psi(\mathbf{u}) &= 0, \text{ in } \mathcal{M}, \\ \int_{\mathcal{M}} |\psi(\mathbf{u})|^2 d\mathcal{M} &= 1, \\ < \nabla\psi(\mathbf{u}), \mathbf{n} >|_{\partial\mathcal{M}} &= 0, \end{aligned} \tag{3}$$

where Δ is the LB operator; $\mathbf{u}$ is the local coordinates with entries u_1 and u_2 on $\mathcal{M}$. $\mathbf{n}$ is the normal vector on the boundary of $\mathcal{M}$. A numerical solution, using a finite element implementation, of this eigenvalue problem is provided in [7].

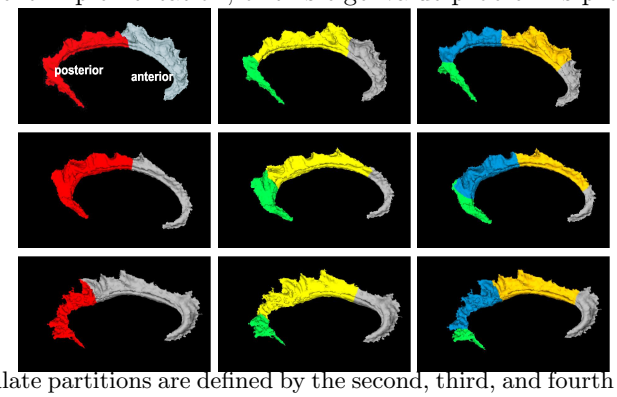

Fig. 3. Cingulate partitions are defined by the second, third, and fourth eigenfunctions. Each row gives cingulate partitions for one subject.

Eigenfunctions are ordered according to increasing eigenvalues. The first eigenfunction is a constant function, corresponding to the zero eigenvalue. Shown in Figure 2 are examples of eigenfunctions generated via the LB operator on three different cortical gyri. The automated partition on the cortical surface subregions is obtain via the nodal domains of the LB eigenfunctions. For instance, the top row in Figure 2 shows examples of the second, third and fourth eigenfunctions on cingulate. The region in red has positive values, while the region in blue has negative values. As one goes to the higher order of eigenfunctions, red and blue regions alternate rapidly. The number of nodal domains is bounded by Courant's nodal theorem and each nodal domain has at least D_j vertices. Such nodal domains are labeled as index j, $1, 2, \cdots$, from anterior to posterior of cingulate. The nodal lines are sets of vertices as the form $\mathcal{L}(\phi_i) = \{v_n : e_{mn} \in \mathcal{M},\ \phi_i(v_m)\phi_i(v_n) < 0 \text{ and } l_m > l_n\}$, where l_m and l_n are labels of the nodal domains that vertices v_m and v_n belong to. e_{mn} is an edge between v_m and v_n on surface M. Figure 3 below illustrates the nodal domains in cingulate gyri generated from the multiple eigenfunctions. The intrinsic methodology associates to each surface a triangular sequence of domains of the form $N_{11}, N_{21}, N_{22}, N_{31}, N_{32}, N_{33}, \ldots, N_{n1}, \ldots, N_{nn}, \ldots$ where $N_{n1}, \ldots, N_{nn}$ is the nodal partictions associated to the nth eigenfunction of the Laplacian. Then the partition functions are characteristic functions of these domains, namely $\psi_{nk}(x) = 1_{N_{nk}}(x)$.

4 Extrinsic Study of Anatomical Coordinates

The previous definition clearly addresses the intrinsicality and locality principle. Like for the random field model, the reliability issue is not as straightforward and can fail to be true for some surfaces. This can be related to possible multiplicity of eigenvalues (see Figure 4) for the Laplacian, which is often associated to symmetries within the manifold.

The extrinsic version of the nodal analysis simply involves carrying the generalized partition from the template onto each of the individual anatomical configurations, according to equation (2).

The correspondences (ϕ) are constructed using Large Deformation Diffeomorphic Metric Mapping methods with landmark data. Landmark data is one among several instances of modalities that can be aligned with LDDMM, together with images, tensors (DTI), unlabelled points and measures, courants and surfaces ... [15–18].

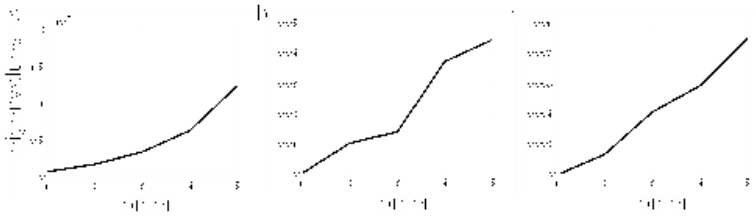

Fig. 4. Panels (a-c) show the first 5 eigenvalues of cingulate, planum temporale, and central sulcus that are shown in Figure 2. Panel (b) shows that the second and third eigenvalues of the planum temporale are close to each other. This evidence is also observed on the second row of Figure 2.

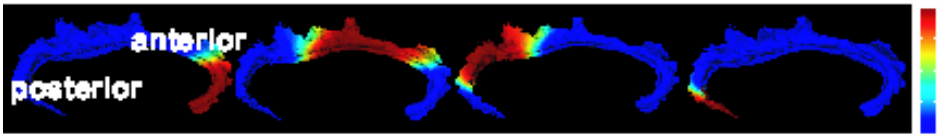

Fig. 5. Probability maps of each region as a function of cortical location.

In this experiment, we work with a database of 113 landmarked cingulates, each of them provided with its own collection of (intrinsic) nodal functions, that will be denoted $\psi_{nk}^{(j)}, n \geq 2, k \leq n$, j indexing the cingulates.

For the extrinsic representation, we selected the cingulate of one healthy subject as template, then used the landmark matching procedure[15, 19] to register the dataset on the template. Letting $\phi^{(j)}$ be the deformation carrying the left (or right) template to the left (or right) cingulate of subject j, the intrinsic nodal functions $\psi_{nk}^{(j)}$ were remapped as $\psi_{nk}^{(j)} \circ \phi^{(j)}$ to the cingulate template. We then measured how each class of remapped domains overlaps by computing, for all points x in each the template.

$$P_{nk}(x) = \frac{1}{J} \sum_{j=1}^{J} \psi_{nk}^{(j)} \circ \phi^{(j)}(x) \ , \ k = 1, \ldots, n \ .$$

Figure 5 shows the probability maps for each nodal domain determined by the fourth LB eigenfunction in the case $n = 4, k = 1, 2, 3, 4$. For instance, the left top panel shows that the region in red certainly belongs to the first nodal domain N_{41} while the region in blue is not in this domain and the region colored from red, yellow, green to blue is the transition region between two nodal domains due to the variation of the brain anatomy across subjects.

5 Statistics in Nodal Domains

When trying to characterize the neuroanatomical and functional abnormalities associated with a specific neuropsychiatric disorder, certain fundamental questions always arise. The most important one is asked to detect group difference in anatomical structure and function of a particular brain region. This can be quite challenging due to highly variable brain structure across subjects and high dimensionality of data (e.g. thickness function defined on the cortical surface) compared to the small number of individuals in each group. Partitioning the cortex into different domains seems a way to overcome these issues by reducing the complexity of brain structure into domains and reducing dimensionality of data. Below we define a statistic corresponding to each nodal domain for detecting group differences.

For a scalar function $F^{(j)}(x)$ defined on cortical surface j, such as cortical thickness, curvature, or functional response, we define the normalized scalar measurement $\overline{F}_{nk}^{(j)}$ within nodal domain $N_{nk}^{(j)}$ by

$$\overline{F}_{nk}^{(j)} = \frac{\int_{\mathcal{M}^{(j)}} F^{(j)}(x)\psi_{nk}^{(j)}(x)ds(x)}{\int_{\mathcal{M}^{(j)}} \psi_{nk}^{(j)}(x)ds(x)} \ , k = 1, 2, \cdots, n \ , \tag{4}$$

where $\psi_{nk}^{(j)}$ is as before the indicator function of domain N_{nk}. Again, $\psi_{nk}^{(j)}$ is computed from individual cortical surface in the intrinsic analysis, while only one set of partition functions $\psi_{nk}^{(atlas)}$ is used in the extrinsic analysis and then transported to the other surfaces via diffeomorphic regsitration. Group difference of $\overline{F}_{nk}^{(j)}$ within each nodal domain is detected to perform statistical analysis, such as t-test, rank sum test.

5.1 Clinical Studies

Extrinsic Study. Our first example discusses the use of the extrinsic random field model (section 2) to characterize group differences of structural or functional measurement on the cortical surface. We give an example of the clinical study in schizophrenia for the subcortical structure – left planum temporale (lPT), which is the associate auditory system located on the left superior temporal gyrus. We have assessed the lPT thickness in 10 healthy subjects, 10 subjects with schizophrenia, matched with age and gender. We first chose one lPT of a healthy subject as template and all others were deformed into the template space using the diffeomorphic surface matching approach [16]. The cortical thickness maps on the other lPTs were then remapped to the template. The

average thickness maps within the healthy and schizophrenic groups are shown in Figure 7(a,b), respectively. These two panels suggest that there are similar patterns in both groups, that is, the lPT is thin at the bottom of Heschl's sulcus (HS), then progressively thicker away from HS, and finally thinner towards the posterior ramus. Figure 7(c) shows pairwise differences in the average thickness maps between the two groups. Red denotes the region where the lPT is thicker in the healthy control group than in the schizophrenic group while blue represents the region where the lPT is thinner in the healthy group than in the schizophrenic group. To demonstrate the group difference, each thickness map was expanded as a linear combination of eigenfunctions shown in Figure 6 with a coefficient vector $f^{(i,j)}$, where i is the index of groups and j is the index of subjects in group i. The Hotelling's T^2 test was incrementally performed on $F^1 = \{f^{(1,j)}, j = 1, 2, \cdots, N\}$ and $F^2 = \{f^{(2,j)}, j = 1, 2, \cdots, N\}$ when $N = 1, 2, 3, \cdots$. We found that the group difference in thickness occurs in the second, third, and fourth eigenfunctions shown in Figure 6(a,b,c), respectively. The significant group difference reconstructed by these eigenfunctions is shown in panel (d) of Figure 7. Several previous studies have shown that reduced superior temporal gyrus volume is associated with hallucinations/delusions or positive formal thought disorder [20]. This with our thickness results thus implies that the region showing thickness decrease relative to healthy comparison controls is associated with these dysfunctions (hallucinations/delusions or positive formal thought disorder).

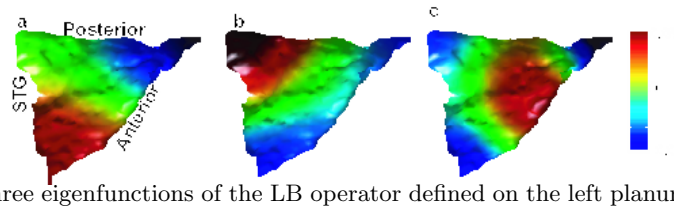

Fig. 6. Three eigenfunctions of the LB operator defined on the left planum temporale.

Intrinsic study. We study the thickness variation of cingulate in schizophrenia using the approach described in Section 5 in the intrinsic analysis. The cingulate gyrus is the part of the cerebrum that lies closest to the limbic system, above the corpus callosum. It provides a pathway from the thalamus to the hippocampus, is responsible for focusing attention on emotionally significant events, and for associating memories to smells and to pain. It has been considered as prominent brain structure related to schizophrenic symptoms. The cortical thickness of the cingulate gyrus estimated from MRI is one of quantitative morphometric measurements, which indirectly implies cellular changes in density as well as soma size and directly indicates the change in gray matter volume and anatomical shape that may be associated with schizophrenia. Figure 8 gives examples of thickness maps of a control and schizophrenic patient. The interesting questions arising are how to detect group difference on the cingulate surface and (if there is one) how to localize such a change on the cingulate surface. To answer these questions, we applied the intrinsic method. Two-sided rank sum tests were performed on the coefficients $\overline{F}_{nk}$ to detect and quantify nonuniform abnormalities

of the cortical thickness on cingulate surfaces in 20 subjects with schizophrenia as compared to 20 healthy subjects matched for gender and age. We found distinct pattern of thickness on the left cingulate gyrus. In terms of power of statistical testing, the most significant change in thickness between healthy and schizophrenic groups is on the region colored in blue shown in the last column of Figure 3. As for the right side of the cingulate gyrus, distinct pattern of thickness is shown in both anterior and posterior segments of the cingulate gyrus as well.

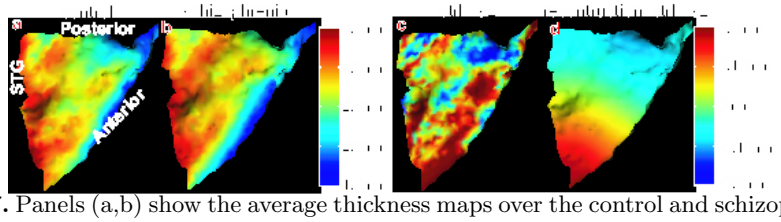

Fig. 7. Panels (a,b) show the average thickness maps over the control and schizophrenic groups on the left planum temporale. Panel (c) shows the difference in thickness between the control and schizophrenic groups. Panel (d) illustrate the significantly different pattern in thickness between these two groups, which is constructed using eigenfunctions shown in Figure 6.

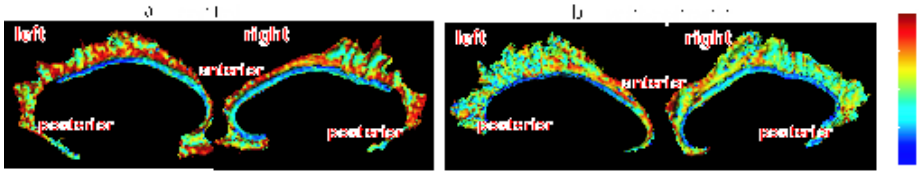

Fig. 8. Panel (a) shows cortical thickness maps on the left and right cingulates of one healthy control subject. Panel (b) shows thickness maps for one schizophrenic patient.

6 Conclusion

This paper presents the intrinsic and extrinsic methods both of which are powerful tools to study statistical inference on physiological random signals F in anatomical coordinates. The extrinsic method has been used to study the anatomical variability in the last decade. An advantage of the extrinsic analysis is that only one set of partition functions is needed for the template coordinate. But this requires to find the correspondence between anatomies that carries these partition functions to each anatomical coordinate. The intrinsic method may become an alternative way to study statistical inference on F across populations if such a correspondence between anatomies is not well defined. The tradeoff of this method is that the set of partition functions has to be found for every anatomical coordinate, which is solved based on Courant's theorem on nodal analysis via the LB operator in this paper.

Acknowledgements

This work was supported by NIH grants: R01 MH 064838, R01 EB00975, P41 RR15241, and P20 MH071616. The authors would like to thanks Dr. Csernansky and Dr. Wang from Washington University in St. Louis for cingulate data,

Dr. Ratnanather and Dr. Barta from the Johns Hopkins University for planum temporale and central sulcus data.

References

1. Grenander, U., Miller, M.I.: Computational anatomy: An emerging discipline. Quarterly of Applied Mathematics **LVI**(4) (1998) 617–694
2. Csernansky, J.G., Joshi, S., Wang, L., Hallerparallel, J.W., Gado, M., Miller, J.P., Grenander, U., Miller, M.I.: Hippocampal morphometry in schizophrenia by high dimensional brain mapping. PNAS **95** (1998) 11406–11411
3. Csernansky, J.G., Wang, L., Joshi, S.C., Ratnanather, J.T., Miller, M.I.: Computational anatomy and neuropsychiatric disease: probabilistic assessment of variation and statistical inference of group difference, hemispheric asymmetry, and time-dependent change. NeuroImage (2004) S139–S150
4. Thompson, P.M., Hayashi, K.M., Sowell, E.R., Gogtay, N., Giedd, J.N., Rapoport, J.L., de Zubicaray, G.I., Janke, A.L., Rose, S.E., Semple, J., Doddrell, D.M., Wang, Y., van Erp, T.G., Cannon, T.D., Toga, A.W.: Mapping cortical change in alzheimer's disease, brain development, and schizophrenia. NeuroImage **23** (2004) S2–S18
5. Van Essen, D.: Surface-based approaches to spatial localization and registration in primate cerebral cortex. NeuroImage **23** (2004) s97–s107
6. Fischl, B., Sereno, M.I., Dale, A.M.: Cortical surface-based analysis II: inflation, flattening, and a surface-based coordinate system. NeuroImage **9** (1999) 195–207
7. Qiu, A., Bitouk, D., Miller, M.I.: Smooth functional and structural maps on the neocortex via orthonormal bases of the Laplace-Beltrami operator. submitted to IEEE transactions on medical imaging (2005)
8. Coifman, R.R., Lafon, S., Lee, A.B., Maggioni, M., Nadler, B., Warner, F., Zucker, S.W.: Geometric diffusions as a tool for harmonic analysis and structure definition of data: Diffusion maps. PNAS **102** (2005) 7426–7431
9. Shi, J., Malik, J.: Normalized cuts and image segmentation. IEEE Tran PAMI **22** (2000) 888–C905
10. Belkin, M., Niyogi, P.: Semi-supervised learning on riemannian manifolds. Machine Learning **56** (2004) 209–239
11. Angenent, S., Haker, S., Tannenbaum, A., Kikinis, R.: Laplace-beltrami operator and brain surface flattening. IEEE Trans. Medical Imaging **18** (1999) 700–711
12. Gu, X., Wang, Y., Chan, T., Thompson, P., Yau, S.: Genus zero surface conformal mapping and its application to brain surface mapping. Information Processing Medical Imaging (2003)
13. Memoli, F., Sapiro, G., Thompson, P.: Implicit brain imaging. NeuroImage **23** (2004) S179–S188
14. Courant, R., Hilbert, D.: Methods of Mathematical Physics. Volume 1. Interscience Publishers, New York and London (1953)
15. Joshi, S.C., Miller, M.I.: Landmark matching via large deformation diffeomorphisms. IEEE Trans. Image Processing **9**(8) (2000) 1357–1370
16. Vaillant, M., Glaunès, J.: Surface matching via currents. Lecture Notes in Comp. Sci.: Inform. Proc. in Med. Imaging **3565** (2005) 381–392
17. Beg, M.F., Miller, M.I., Trouvé, A., Younes, L.: Computing large deformation metric mappings via geodesic flows of diffeomorphisms. International Journal of Computer Vision **61**(2) (2005) 139–157

18. Cao, Y., Miller, M., Winslow, R., Younes, L.: Large deformation diffeomorphic metric mapping of vector fields. IEEE Trans. Med. Imag. **24** (2005) 1216–1230
19. Allassonnière, S., Trouvé, A., Younes, L.: Geodesic shooting and diffeomorphic matching via textured meshes. In: EMMCVPR. (2005) 365–381
20. Shenton, M.E., Dickey, C.C., Frumin, M., McCarley, R.W.: A review of MRI findings in schizophrenia. Schizophr Res. **49** (2001) 1–52